ENA detection in the dayside of Mars: ASPERA-3 NPD statistical study

A. Mura[a], S. Orsini[a], A. Milillo[a], E. Kallio[b], A. Galli[c], S. Barabash[d], P. Wurz[c], A. Grigoriev[d], Y. Futaana[d], M. Holmström[d], H. Andersson[d], R. Lundin[d], M. Yamauchi[d], M. Fraenz[e,] N. Krupp[e], J. Woch[e], K. Asamura[f], A. J. Coates[g], C. C. Curtis[h], K. C. Hsieh[h], B. R. Sandel[h], A. Fedorov[i], M. Grande[j], H. Koskinen[k], J. U. Kozyra[l], J. G. Luhmann[m], S. McKenna-Lawlor[n], R. Cerulli-Irelli[a], R. D'Amicis[a], M. Maggi[a], S. Massetti[a], E. C. Roelof[n], P. C. Brandt[o], K. Szego[p], D. J. Winningham[q], R. A. Frahm[q,] J. R. Sharber[q].

[a] Instituto di Fisica dello Spazio Interplanetario, Rome, Italy
[b] Finnish Meteorological Institute, Helsinki, Finland
[c] Physikalisches Institut, University of Bern, Bern, Switzerland
[d] Swedish Institute of Space Physics, Kiruna, Sweden
[e] Max-Planck Institut fur Sonnensystemforschung, Katlenburg-Lindau, Germany
[f] Institute of Space and Astronautical Science, Sagamichara, Japan
[g] Mullard Space Science Laboratory, University College London, UK
[h] University of Arizona, Tucson, USA
[i] Centre d'Etude Spatiale des Rayonnements, Toulouse, France
[j] University of Wales, Aberystwyth, UK
[k] University of Helsinki, Helsinki, Finland
[l] Space Physics Research Laboratory, University of Michigan, Ann Arbor, USA
[m] Space Science Laboratory, University of California in Berkeley, Berkeley, USA
[n] Space Technology Ltd., National University of Ireland, Maynooth, Ireland
[o] Applied Physics Laboratory, Johns Hopkins University, Laurel, USA
[p] KFKI Research Institute for Particle and Nuclear Physics, Budapest, Hungary
[q] Southwest Research Institute, San Antonio, USA

Abstract. The Analyzer of Space Plasma and EneRgetic Atoms (ASPERA-3) instrument suite on board Mars Express is designed to study the interaction between the solar wind and the atmosphere of Mars and to characterize the plasma and neutral gas environment in near-Mars space. Neutral Particle Detectors (NPD-1 and 2), part of the ASPERA-3 package, are Energetic Neutral Atom (ENA) detectors which use the Time-of-flight (ToF) technique to resolve the energy of detected particles. Pulse-height analysis is used to distinguish between hydrogen and oxygen. In the present study we perform a statistical analysis of NPD ToF data collected between 14-Mar-2004 and 17-Jun-2004. We have restricted our data-set to the dayside of Mars. These data are pre-processed to remove UV contamination. ToF spectra are fitted with simple analytical functions to obtain a set of parameters. The behavior of these parameters, as a function of spacecraft (s/c) position and attitude, is investigated and reveals the existence of an ENA signal, interpreted to probably coming from charge-exchange of shocked solar wind protons on the dayside of Mars at <1000 km above the planetary surface.

1 Introduction

Energetic Neutral Atoms (ENAs) originate in the neutralization of energetic plasma by exospheric gasses; in this process, called *charge-exchange*, an incoming ion catches an electron from the ambient neutral gas; the newly formed neutral (ENA) retains (approximately) both the energy and direction of the incoming ion. Since ENAs are no longer affected by electromagnetic fields, they travel along straight lines just like photons; their detection is, thus, usually referred to as "ENA imaging". This technique is a useful way: i) to remotely and globally study the property of the source plasma and ii) to study the interaction between neutral particles and space plasma (Roelof and Williams, 1985).

The ESA mission Mars Express carries a plasma and neutral particle package, the Analyzer of Space Plasma and Energetic Atoms (ASPERA-3) (Barabash *et al.*, 2004). ASPERA-3 includes four sensors; the Neutral Particle Detectors (NPD1 and 2), in particular, is a neutral mass analyzer, and can resolve particle velocities and masses with low angular resolution.

Since the solar wind (SW) interacts with Mars mainly through direct impact with its ambient atmospheric/exospheric gas (Kallio *et al.,* 1997), charge-exchange is expected to be very effective there. ENA imaging is, hence, a potentially useful tool to allow insight into the geometry, the physics, and the dynamics of the plasma around Mars.

Here we present a statistical study of NPD Time of Flight (ToF) data, collected on the dayside of Mars during three months of 2004. In this frame, at least two different sources of ENAs were identified: namely ENA albedo and ENA jets (Futaana *et al.*, 2006a, 2006b). ENA albedo is produced when charge-exchange ENAs are generated above the Induced Magnetosphere Boundary (IMB; Lundin *et al.*, 2004), cross the IMB and are back-scattered against the exobase (Kallio and Barabash, 2001). A fraction of SW protons cross the IMB due to finite Larmor radius effect and experience a back-scattering process (proton-ENA albedo, Holmström *et al.*, 2002), thereby potentially contributing to the overall signal. In addition, spatially constrained and highly directional ENA fluxes (ENA jets) up to 7×10^5 cm^{-2} sr^{-1} s^{-1}, in the 0.3-3 keV energy range, emanating from a compact region of the sub-solar exosphere, have been detected by the NPD (Futaana *et al.*, 2006b).

In section 2, we briefly describe the NPD instrument and the present data set. A photon noise contamination reduction technique is described in section 3. Data analysis is discussed in section 4, the results in section 5 and a summary is given in section 6.

2 Instrument and data set

NPD is a pinhole camera acting as a mass and energy spectrometer with raw angular resolution of 5°×40°. ENAs are collimated and discriminated from ions by a pair of charged plates. They then hit a start surface at grazing angles and the detection of the emitted electrons gives the *start* signal. The reflected ENAs travel inside a ToF chamber and then hit a *stop* surface, thereby providing the ToF measurement (Barabash *et al.,* 2004). Two NPD units are included in ASPERA-3, pointing in different directions; the 6 sectors cover a global Field of View (FoV) of 5°×180°.

We have analyzed the NPD (BIN mode) data recorded by both units in the time period from 14-Mar-2004 to 17-Jun-2004, on the dayside of Mars. The mass resolution of the instrument (coming from pulse-height analysis of the *stop* signal) has not been utilized; the data have been "downsampled" to a time resolution of 30 s thought integration (to decrease the inherent noise); for each 30 s time interval, a 16-channel ToF spectrum has been obtained. Using these ToF values we calculate the energy-per-nucleon (for simplicity, in what follows, we will refer to this just as "energy"), assuming a ToF path of 8 cm. The s/c was in "nadir" mode, and sectors 0 of NPD1 and NPD2 (NPD1-0 and NPD2-0) always pointed towards Mars. All other sectors, and especially those of the NPD2, where always pointing away from the sun; none was pointing completely away from the planetary environment where the ENA flux is expected to be generated.

3 UV filtering

UV suppression in the NPD is based on the coating of the start surface (to minimize UV efficiency) and on the coincidence of start/stop signals. However, the instrument is still sensitive to UV and several post-acquisition UV suppression methods have been proposed (see for example, Futaana et al., 2006b, Galli et al., 2007). Here, we have assumed that the highest ToF channel contains only false (UV) counts and no real data. In fact, for H, this channel corresponds to an energy of ~10 eV, too low to be detected by the stop MCPs (conversely, for O, the corresponding energy is ~200 eV, so that counts could constitute a real ENA signal). The UV count rate for all other ToF channels can be calculated as in the following: we assume that some photons cause false start and stop signals with frequencies (respectively) F and F^*, where $F=kF^*$ and $k>>1$. The ToF distribution of these false events is: $f(ToF)=F\,e^{-F\,ToF}$. The total number of UV false counts, N_{tot}, is equal to $T_{acc}\,F^*$; the number of UV false counts N_{ij} between ToF_i and ToF_j is:

$$N_{ij} = N_{tot}\int_{ToFi}^{ToF_j} Fe^{-F\,ToF}\,dToF = T_{acc}\frac{F}{k}\int_{ToF_i}^{ToF_j} Fe^{-F\,ToF}\,dToF = -T_{acc}\frac{F}{k}\left(e^{-F\,ToF_j} - e^{-F\,ToF_i}\right). \quad (1)$$

To obtain F from this equation we calculate the Maclaurin expansion; and in the first order we have:

$$F = \sqrt{\frac{kN_{ij}}{T_{acc}\left(ToF_j - ToF_i\right)}}\,; \quad (2)$$

k is ~ 30 (Fuutana et al., 2006b); however, this parameter disappears in the final equation (in the first order only). Here we have used the last channel (ToF_i = 1514 ns, ToF_j=1900 ns) to calculate F; then we have calculated N for the other channels and subtracted it from the (related) measured count rates. It is worth noting that, assuming only H-ENA, it is safe to also use the last two or three channels (E < 40 eV). In fact, in a preliminary test we have used a similar procedure with the last two channels obtaining same values for F. An example of NPD data before and after UV contamination removal is shown in fig. 1.

4 Data analysis

The purpose of the present study is to provide a statistical characterization of the ENA signal recorded on the dayside of Mars. With this in mind, we have fitted every spectrum using a simple analytical function. To allow the detection of different ENA sources, we have used the sum of two gaussian functions (peaking at different energies: p_1 and p_2):

$$f(E) = A_1 e^{-\frac{(\log(E)-p_1)^2}{2\sigma_1^2}} + A_2 e^{-\frac{(\log(E)-p_2)^2}{2\sigma_2^2}} \quad ,(3)$$

where $x=\log_{10}(E)$; $A_{1/2}$, $p_{1/2}$, and $\sigma_{1/2}$ are free parameters. To preserve the original statistical weight of the count rate of each channel, we have decided to apply this procedure directly to the raw data N_{ij} and not to the energy spectra $N(E)=N_{ij}/\Delta E$; otherwise, the values (and the weight during the fitting procedure) of the low-energy channels would be increased more, because ΔE is smaller. Since the ToF/energy channels are logarithmically spaced (i.e. $\Delta E \sim E$), a gaussian function has the advantage that it remains a gaussian function when describing the energy spectrum (i.e. after dividing by ΔE). The coefficients can be adjusted: for example, the new peak position is:

$$p' = p - \log(10)\,\sigma^2. \quad (4)$$

We have placed no constraints on the position of p_1 and p_2, except $p_1 < p_2$. However, we have decided to discard all those spectra that looked "suspect" in any way, for example, those spectra where a single channel displayed an unreasonably high value. The total number of spectra to be processed (S) after this phase, was ~ $3\ 10^4$, depending on the considered sector. The number of valid spectra for sector NPD1-0 was too low and, for this reason, data from this sector have been excluded from this study. The spatial statistical coverage of the valid data can be deduced from figure 2; most of the data have been collected at a planetocentric distance (r) between 1.5 and 2 Mars' radii (R_M, ~3400 km) and at an angle (α) from the Sub-Solar Point (SSP) between 40° and 70°. After the best-fit procedure (least squares method), we have obtained an array of S values for each of the 6 free parameters: A_1, p_1, σ_1, A_2, p_2, and σ_2. Due to the absence of an intrinsic, global magnetic field (Dolginov, 1978; Acuna *et al.*, 1998), we can assume, as a first approximation, that the plasma flows around the planet, and hence the ENA distribution, has a cylindrical symmetry, assuming that the possible influence of the IMF is smoothed out in our statistical study. Hence, we have defined a cylindrical coordinate system: (x from Mars' center to Sun; h perpendicular to x), with a resolution of 0.1 R_M. Taking into account the average s/c velocity, the time-window (30 s) corresponds to less than 100 km; hence, the temporal integration does not affect our spatial resolution significantly. Next, we have calculated the mean value of each parameter within each grid cell and for each sector. In figure 2 we show the results from this procedure in terms of pseudo-colour maps of the amplitudes of the high- and low-energy gaussian functions. The widths σ_1 and σ_2 are approximately uniform and between 0.6 (σ_1) and 0.7 (σ_2) (in logarithmic scale) with p_1 around 100 eV and p_2 around 1000 eV (only where A_2 is relevant).

5 Interpretation of data

We start this section with a brief discussion of the low-energy signal. At this preliminary stage of analysis it appears that, in principle, two different sources of ENA signals have been revealed. This possibility is suggested by the fact that the fitted amplitudes (fig. 2, left panel) show some correlation with the sensor position and with the sector attitude.

However, the low-energy peak position, (p_2', adjusted with eq. 4), is well below 100 eV/amu. Assuming hydrogen ENAs, such an energy is too low to be detected by the NPD. Of course, it is possible to hypothesize the presence of heavy ENAs from planetary ions (like oxygen), but it seems that the count rate (up to 20 s^{-1}, which is similar to the high-energy case, see below) is too high. On the other hand, there are strong indications that this signal can be due to UV contamination. If we consider NPD2-0, for example, we notice that the low-energy amplitude (fig. 2, panel A) is inversely proportional to h. This sector points approximately in the anti-sunward direction, so that the UV albedo flux should be approximately proportional to the fraction of planetary surface inside the sector FoV.

We next discuss the high-energy signal. Even though the sector count rates are not inter-calibrated, it is possible to assume, as a zero-order hypothesis, that the relative count rates reflect the relative incoming flux. Under this assumption, the detected count rate is higher in NPD1-1 and -2, which look towards the SSP. The 30-s averaged count rate is up to 20 s^{-1} and is inversely proportional to the s/c height. The energy of this peak is approximately uniform and of the order of 1 keV. By applying eq. 4 we can estimate that, on average, the energy spectra peak between 100 eV and 500 eV. If we consider NPD1 sector 1, the count rate decreases with increasing distance (r) from ~ 20 at 1.5 R_M to below 10 at 2 R_M. On the other hand, there is no evident correlation with the angle α. A simple best-fit of the ENA count rate shows that it is approximately proportional to $r^{-2.1}$. Hence, these observations are consistent with an ENA source located close to the planetary surface and emitting an isotropic flux, which is supposed to decrease as $\sim r^{-2}$. Assuming such a source, NPD1 sec. 2 points towards this ENA generation region only when the s/c distance r is small (i.e. ~1.5 R_M). In fact, in this case the count rate decrease with r is somewhat more pronounced and approximately proportional to r^{-3}. Moreover, the flux is highest for those sectors pointing towards the sub-solar region (NPD1-1 and NPD1-2), very low for those partially looking towards the dayside (NPD2, sec. 0 and 1) and close to zero for NPD2-2, which looks away from the SSP.

To investigate the hypothesis that the charge exchange of shocked solar wind protons with the exosphere (Holmström *et al.,* 2002) generates the features observed, we have performed a simulation of the expected signal using the ENA simulation model of Mura *et al.* (2002). This model uses an analytical description of the H^+ flow around the planet (velocity, density and temperature; Kallio, 1996) and the exospheric profiles of H, H_2 and O of Krasnopolsky and Gladstone (1996). To take into account recent observations of smaller exospheric profiles (Galli *et al.*, 2007), we have reduced them by a factor of 10. For each sector and for each of the S spectra, we have computed the simulated ENA signal at 500 eV (which is approximately the energy of the detected signal) taking into account the real s/c position and instrument attitude and using a *line of sight* integration technique. Then we have calculated the estimated count rate for NPD using the instrument geometrical factor (5 10^{-5}, Grigoriev *et al.*, 2003) and the channel size. In this way, we have deduced the expected values ($\overline{A}_2$) of the parameter A_2 (high-energy peak amplitude), which we then have compared with the experimental values. Moreover, we have estimated the UV (un-calibrated) inside the instrument by using a simulation similar to that of Brinkfeld *et al.* (2006); i.e. we have considered the UV isotropic scattering using the adopted exospheric model (but without a realistic calibration coefficient or cross sections, since we are only interested in the spatial distribution). The UV rate is in arbitrary units. In figure 3 we show the distribution of the parameter A_2 (panel A), for all sectors together, as a function of the angle between the FoV direction and a point P located at (1.2, 0, 0 R_M) (x axis), and of the distance from P (y axis). The distribution of

simulated parameter $\overline{A}_2$ is shown in panel B. For consistency, in the same figure and using the same reference frame, we show the distribution of parameter A_1 (panel C) and the distribution of simulated UV (panel D). The point *P* is chosen in order to represent an ENA source region located on the dayside of the planet, close to the surface (of course, the actual source is not restricted to a point). Moreover, the position of *P* is arbitrary within a certain range. We have found that results similar to those shown in figure 3 can be obtained by locating *P* anywhere between 1.1 and 1.5 R_M, i.e. there is i8n this range good agreement between the experimental values (panel A) and the simulated values (panel B).

We have considered the possibility of data contamination due to "pseudo-ENAs", coming from neutralization of ions in the entrance system. Such ENAs have been observed, for example, by the replica instrument ASPERA-4 NPD on board Venus Express during the cruise phase to Venus (A. Galli and M. Fraenz, private communication). However, they have not been observed in similar circumstances by ASPERA-3 NPD. Moreover, such a contamination, if present, should be highest in NPD1-2 (see figure 2), which points approximately against the plasma flux direction in the observation region, while the data show a maximum in NPD1-1.

The possibility of a residual, partial UV contamination must be considered as well. However, it should be noted that there are at least three other arguments against the hypothesis that UV contamination may dominate.

- The average values of the count rates agree with the estimations (fig. 3, panels A and B).
- The distribution of the simulated UV (panel D) is very similar to that of the low-energy amplitude (A_1, panel C), and conversely, it substantially differs from that of the high-energy amplitude A_2. This fact indicates that: i) A_2 is the intensity of a real ENA signal and ii) A_1 can be presently ascribed only to residual UV contamination. (The UV albedo from the planet has also been considered separately; this distribution -not shown- is very similar to that of fig. 3, panel D, but it is more concentrated around 50°.)
- If we assume that the distribution shown by the right panel of figure 2 (low-energy peak) is due to UV contamination, then the distribution shown by the left panel (high-energy peak) substantially differs and cannot be ascribed to the same source.

6 Concluding remarks

In summary, we have shown that the major candidate for explaining the detected ENA signal at Mars is charge-exchange of solar wind downstream of the bow shock, and that the results are in good agreement with theoretical predictions. The detected flux may exceed$\cdot 10^5$ cm^{-2} sr^{-1} s^{-1}.

The analysis technique described here is able to give a spatial and energy characterization of the ENA signal detected by ASPERA-3 NPD on the dayside of Mars. We have shown the application of this method using a limited data-set (three months of observations in 2004); in the future, we will extend the time period so as to include all the available data; moreover, the use of an energy-dependent calibration constant will allow a better energy description of the detected signal to be achieved.

Acknowledgement We thank all the national space agencies and those various departments and institutes that collaborates to the ASPERA-3 experiment on board the ESA (European Space Agency) mission Mars Express, and, in particular, the Italian Space Agency (ASI) for supporting our activity. NASA supported US contribution under contract NASW 0003.

References

Acuna, M. H., J. E. P. Connerney, P. Wasilewski, et al., Magnetic field and plasma observations at Mars: Initial results of the Mars Global Surveyor mission, Science, 279, 1676–1680, 1998.

Barabash, S., R. Lundin, H. Andersson, et al. ASPERA-3: Analyser of space plasmas and energetic ions for Mars Express, in Mars Expresss: The scientific payload, vol. SP-1240, edited by A. Wilson, pp. 121–139, ESA Special Publication, 2004.

Brinkfeld, K., et al., First ENA observations at Mars: Solar-wind ENAs on the nightside, Icarus, 182(2), 439-447, 2006.

Dolginov, S. S., On the magnetic-field of Mars - Mars-5 evidence, Geophys. Res. Lett., 5 (1), 93–95, 1978.

Futaana, Y., S. Barabash, A. Grigoriev, et al., First observation of ena emissions from the martian upper atmosphere, Icarus, 182, 424-430, 2006a.

Futaana, Y., A. Grigoriev, S. Barabash, et al., Subsolar ENA jet at Mars, Icarus, 182, 413-423, 2006b.

Galli, A., P. Wurz, H. Lammer, H.I.M. Lichtenegger, R. Lundin, S. Barabash, A. Grigoriev, M. Holmström, and H. Gunell, The Hydrogen Exospheric Density Profile Measured with ASPERA-3/NPD, Space Science Rev. 2007.

Grigoriev, A., S. Barabash, A. Fedorov, MarsExpress ASPERA-3 NPD FM2 calibration report, March 18, 2003

Holmström, M., S. Barabash, and E. Kallio, Energetic neutral atoms at Mars: I. Imaging of solar wind protons. J. Geophys. Res., 107 (A10), 1277, 2002.

Kallio, E. An empirical model of the solar wind flow around Mars, J. Geophys. Res., 101, 11133, 1996.

Kallio, E., and S. Barabash. Atmospheric effects of precipitation energetic hydrogen atoms on the Martian atmosphere, J. Geophys. Res., 106 (A1), 165–177, 2001.

Kallio, E., J.G. Luhmann, and S. Barabash, Charge exchange near Mars, The solar wind absorption and energetic neutral atom production, J. Geophys. Res., 102, 22183, 1997.

Krasnopolsky, V. A., and G. R. Gladstone. Helium on Mars: EUVE and PHOBOS data and implications for Mars' evolution, J. Geophys. Res., 101, 11,765, 1996.

Lundin, R., S. Barabash, H. Andersson, et al., Solar wind-induced atmospheric erosion at Mars: First results from ASPERA-3 on Mars Express, Science, 305, 1933–1936, 2004.

Mura, A., A. Milillo, and S. Orsini. Energetic neutral atoms at Mars: 2. Imaging of the solar wind-Phobos interaction, J. Geophys. Res., 107 (A10), 1278, 2002.

Roelof, E. C., and D. J. Williams, The terrestrial ring current: from in situ measurement to global images using energetic neutral atoms, John Hopkins APL Techn. Dig., 9, 144, 1988.

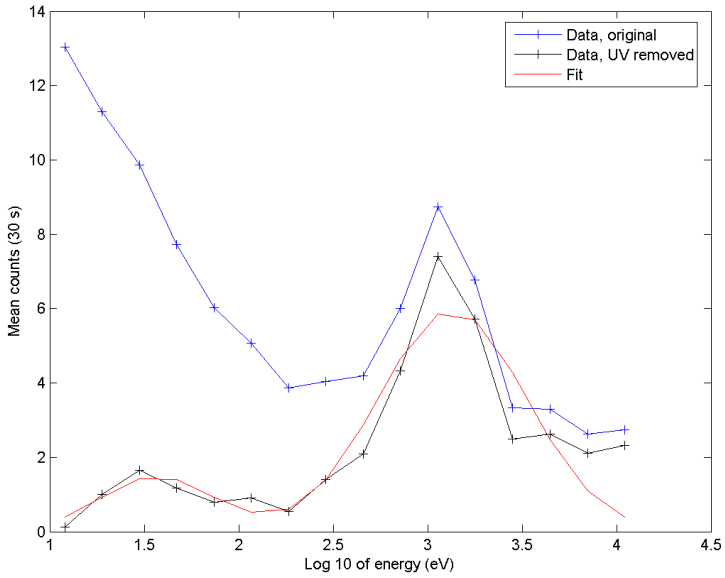

Figure 1: example of data fit, made on raw data. Blue line: unfiltered raw counts; black line: UV-filtered data; red line: best fit.

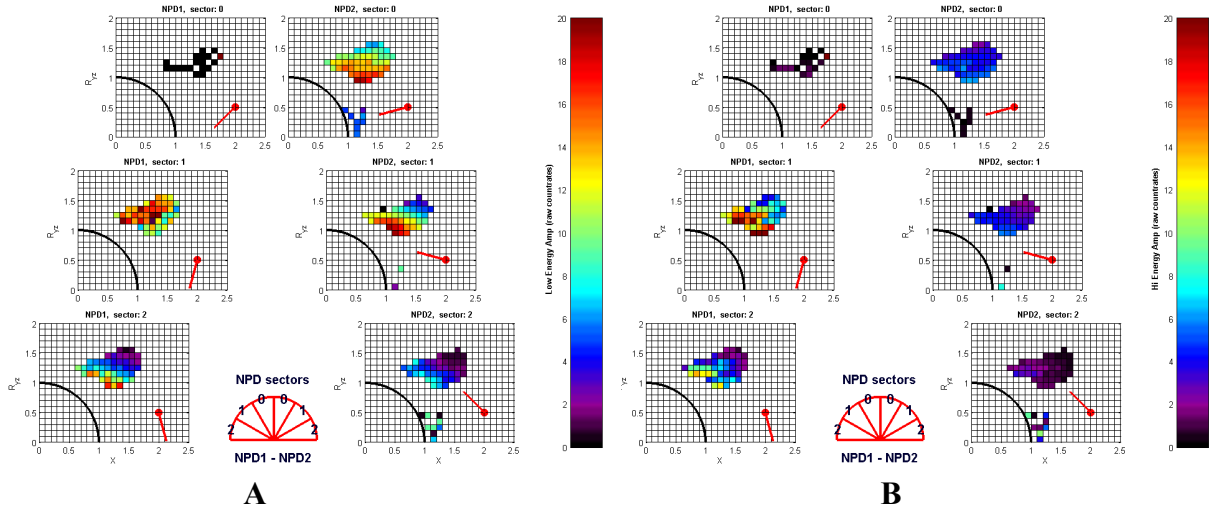

Figure 2. Left panel: pseudo-color maps, in cylindrical coordinates, of the amplitude of the low-energy gaussian function A_1. The color is coded according to the mean value inside a cell o 0.1×0.1 (in Mars' radii). Right panel: same for the amplitude of the high-energy gaussian function, A_2. White cells have no statistical coverage.

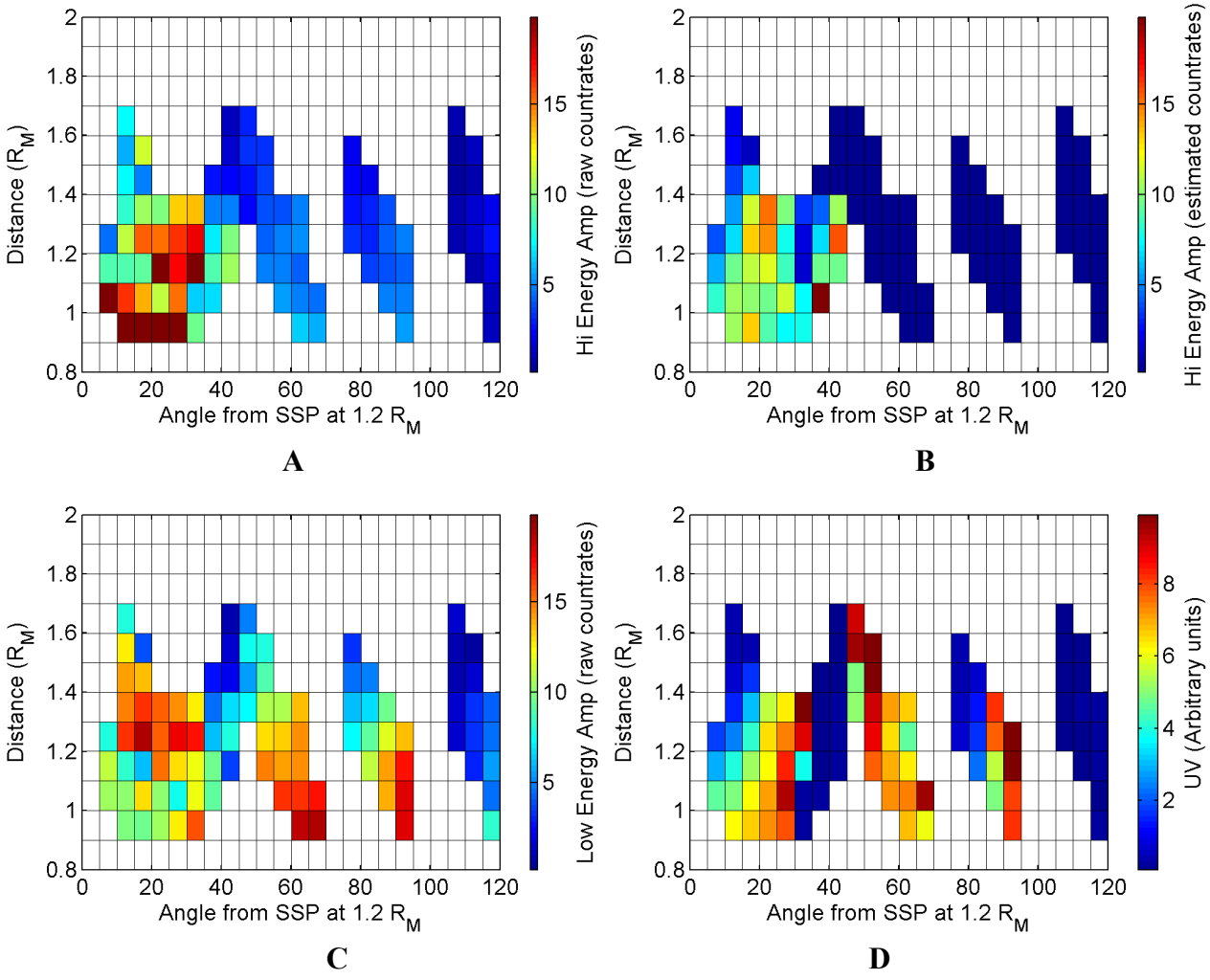

Figure 3. Panel A: pseudo-color map of the high-energy amplitude A_2, as a function of the angle between the FoV direction and the point P (1.2, 0, 0 R_M) (x axis), and of the distance from P (y axis). Panel B: simulation (see text for more details). Panel C: same as panel A, but for low-energy amplitude A_1. Panel D: simulation of UV contamination due to exospheric isotropic scattering; simplified model considering the exospheric model previously applied and using arbitrary "UV to count rate" conversion factor and arbitrary scattering cross section.